

Low field magnetic resonance images of polarized noble gases obtained with a dc superconducting quantum interference device

Matthew P. Augustine,^{a)} Annjoe Wong-Foy, Jeffery L. Yarger, Marco Tomaselli, and Alexander Pines

Materials Sciences Division, Lawrence Berkeley National Laboratory, Berkeley, California 94720 and Department of Chemistry, University of California, Berkeley, California 94720

Dinh M. TonThat and John Clarke

Materials Sciences Division, Lawrence Berkeley National Laboratory, Berkeley, California 94720 and Department of Physics, University of California, Berkeley, California 94720

(Received 7 January 1998; accepted for publication 5 February 1998)

Using a low transition temperature superconducting quantum interference device as a detector, we have obtained magnetic resonance images of laser-polarized ^3He gas and solid ^{129}Xe at 4.2 K in magnetic fields as low as 0.54 mT (^3He) and 1 mT (^{129}Xe), corresponding to Larmor frequencies of 17.6 and 11.8 kHz, respectively. The experimental resolution of the images is $\sim 500 \mu\text{m}$ for ^3He in the gas phase and $\sim 950 \mu\text{m}$ for ^{129}Xe in the solid state. © 1998 American Institute of Physics. [S0003-6951(98)02514-5]

Magnetic resonance imaging (MRI) is a powerful tool in contemporary medical diagnostics¹⁻³ and materials characterization.⁴ The required magnetic fields, B_0 , ranging from 0.1 to 8 T, are often provided by superconducting magnets and lead to Larmor frequencies $\omega_0/2\pi$ of 5–400 MHz. Even at the higher frequency the equilibrium spin population at room temperature, $\hbar\omega_0/k_B T$, is only 6×10^{-5} . In the conventional method of detecting nuclear magnetic resonance (NMR) signals, the voltage across the tuned circuit is proportional to both the polarization and the frequency, that is, to B_0^2 or ω_0^2 . Thus, higher fields normally enhance the sensitivity of NMR/MRI detection. An alternative approach enabling one to obtain images at much lower frequencies is to use a dc superconducting quantum interference device (SQUID) based amplifier to detect the voltages induced in a resonant circuit involving a superconducting inductor.^{5,6} Kumar *et al.*⁵ reported SQUID-detected proton MRIs in fields as low as 9.4 mT, corresponding to a Larmor frequency of about 400 kHz. Such low magnetic fields can be produced relatively inexpensively and have much lower homogeneity requirements compared with high field magnets.

In this letter we describe a second method of improving the detection of low frequency MRI signals, namely the enhancement of the nuclear polarization in low fields by means of optical pumping.⁷⁻⁹ Even in low magnetic field, optical pumping can produce spin polarizations between 10^{-1} and 1 for the noble gases ^3He and ^{129}Xe , an enhancement of several orders of magnitude over their thermal equilibrium polarizations at room temperature in high magnetic field. The enhanced polarization makes the noble gases attractive candidates for use as localized MRI contrast agents.¹⁰⁻¹⁵ We have previously reported¹⁶ the use of a SQUID with an untuned, superconducting input circuit to detect NMR signals from laser-polarized ^{129}Xe in fields down to 0.02 mT, corresponding to a Larmor frequency of 220 Hz. In the present work, optical pumping and SQUID detection are combined

to perform MRIs at 4.2 K and at frequencies as low as 11 kHz.

High spin polarization in ^{129}Xe and ^3He is induced by spin exchange of the noble gas with optically pumped Rb metal vapor.^{8,9} The cylindrical pumping cell typically contains 1 bar of noble gas, 13 mbar of N_2 gas, and a few milligrams of Rb metal. The cell is maintained at 470 K and its contents are irradiated with 1 W of circularly polarized laser light at 794.74 nm, the frequency of the Rb D_1 optical transition, along the direction of a 5 mT magnetic field. This process orients the Rb electron spins parallel to the magnetic field, and results in a polarization of the ^{129}Xe or ^3He nuclear spins to several percent within a few minutes. Since details of the transfer of the sample from the optical pumping station to the SQUID imaging probe at 4.2 K and of the design and operation of the pulsed-SQUID amplifier and its associated electronics are detailed elsewhere,^{16,17} we describe only the probe assembly used in this study.

The sample tube, immersed in liquid ^4He , is placed at the center of a pair of coils, each with a rectangular shape (65×24 mm) and wound with 30 turns of superconducting Nb wire. This coil supplies the static magnetic field \mathbf{B}_0 (Fig. 1). A second pair of coils, each with a rectangular shape (63×20 mm) and with five turns of Nb wire, has a common axis with the \mathbf{B}_0 -field coils and provides the magnetic field gradient \mathbf{G} . The magnetic signal produced by the precessing nuclei is coupled into a two-turn, Nb-wire solenoid with its axis concentric with the cylindrical sample. The pickup coil is connected to the 48-turn, thin-film input coil of the SQUID; the estimated inductances of the two coils, 150 and 200 nH, respectively, are approximately matched. The input circuit forms a superconducting flux transformer, so that the SQUID measures magnetic flux directly rather than the rate of change of flux. The SQUID is operated in a flux-locked loop which has a bandwidth of approximately 5 MHz. The audio-frequency (af) transmitter coil is orthogonal to the pickup coil and static field coils, and consists of two planar 20-turn coils positioned 15.6 mm apart. The static magnetic field and gradient coils are orthogonal to both the af coil and

^{a)}Present address: Department of Chemistry, University of California, Davis, CA 95616.

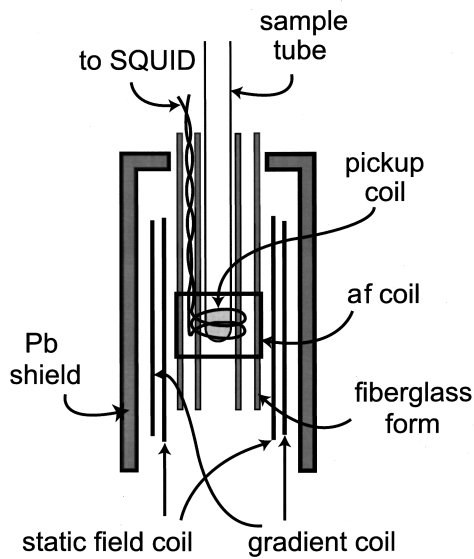


FIG. 1. Configuration of the probe assembly used to obtain ^3He and ^{129}Xe magnetic resonance images at magnetic fields ≤ 1 mT.

the pickup coil and are operated in a persistent-current mode using two separate superconducting switches. In this way a magnetic field up to 1.5 mT and field gradient up to 0.1 T/m can be applied. Because the input circuit has a response that extends to zero frequency, it is surrounded by the superconducting Pb shield shown in Fig. 1 in order to exclude ambient magnetic noise. The shield reduces the static and gradient fields significantly below the values calculated from the geometry of the coils driven by a current ranging from 0.5 to 3 A. To calibrate the static field and gradient coils and to test the ability of the system to obtain an image, a series of experiments was performed first on ^3He gas.

One-dimensional (1D) images of ^3He gas were obtained using a two-pulse spin echo sequence.¹⁸ A typical echo response is shown in Fig. 2 for laser-polarized ^3He gas ($\sim 10\%$ spin polarization) contained in a tube of inner diameter $d = 5.9$ mm at a pressure of 13 mbar. The two af pulses (each consisted of one cycle at a frequency $\omega_{af}/2\pi = 17.6$ kHz and with an amplitude of 0.09 mT) were separated by 0.66 ms, leading to a refocusing of the magnetization at 1.32 ms.

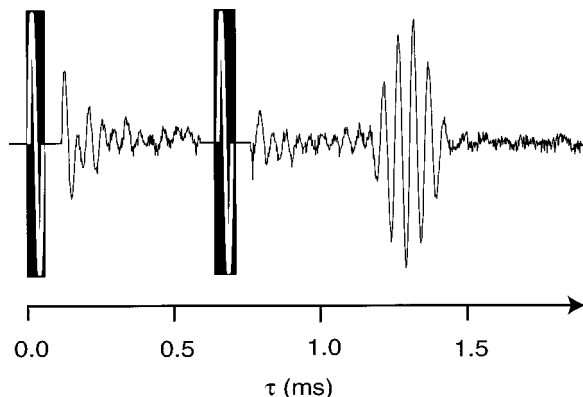


FIG. 2. Spin echo obtained for ^3He at 0.54 mT in a gradient of 0.046 T/m. Each excitation pulse (denoted as a black box in the figure) consists of one cycle at $\omega_{af}/2\pi = 17.6$ kHz with an amplitude of 0.09 mT giving a tipping angle of 61° . The two pulses are separated by 0.66 ms. The receiver-gating time following each pulse is 61 μs .

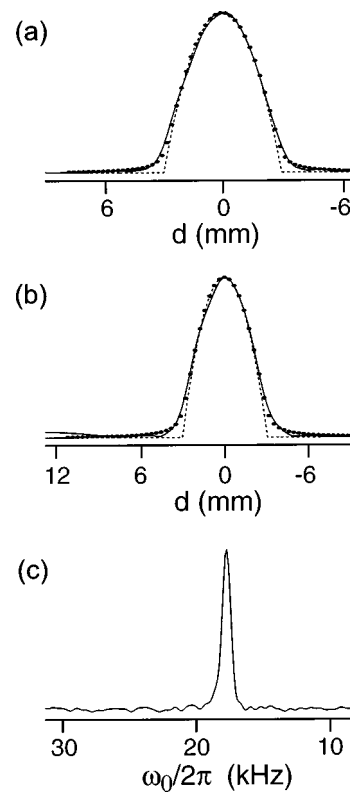


FIG. 3. Solid curves: ^3He spectra as a function of magnetic field gradient for the same static field of 0.54 mT. The abscissa in (c) provides the same frequency scale for all three figures. The abscissa in (a) and (b) provide the spatial scales for these two figures. (a) and (b) Fourier transforms of the signals following the second af pulse with $G = 0.046$ and 0.033 T/m, respectively; in (c), $G = 0$. The dashed lines in (a) and (b) represent the shape of one-half of the circular sample tube. The points in (a) and (b) are the result of the fit to Eq. (2).

Apodization of the echo signal with a hyperbolic secant centered at 1.32 ms and with a width of 1.5 ms, followed by Fourier transformation, yields the spectra shown in Fig. 3. In each spectrum the static field was produced by a current of 1 A, and from the center of gravity of each line and the magnetogyric ratio $\gamma = 32.43$ kHz/mT of ^3He we infer $B_0 = 0.54$ mT. The gradient fields in Figs. 3(a) and 3(b) were produced by currents of 3.0 and 2.0 A, respectively. In Fig. 3(c), the applied gradient field was zero; the observed linewidth is most likely due to the inhomogeneity of \mathbf{B}_0 , although the relaxation times T_1 and T_2 of ^3He gas were not measured in this study. The ^3He images do not show the enhancement at the edges of the tube reported recently by Saam *et al.*¹⁹ in a room temperature ^3He sample at a higher field of 3.1 mT and a smaller gradient of 0.001 T/m. This enhancement arises because the diffusion rate of the gas near the walls is lower than in the interior of the cell.^{20,21} In our case, the lower temperature reduces the diffusion rate, and a lower spatial resolution due to field inhomogeneity blurs features near the edges of the image.

We show that the shapes of the ^3He spectra in Fig. 3 are consistent with the circular distribution function, $\rho(\Omega)$, expected for a linear gradient perpendicular to the symmetry axis of a cylindrical sample, and fit them to find the value of the gradients. The distribution of frequencies in the tube as

$$\rho(\Omega) = \begin{cases} (\Omega_0^2 - \Omega^2)^{1/2} & |\Omega| \leq \Omega_0, \\ 0, & |\Omega| > \Omega_0. \end{cases} \quad (1)$$

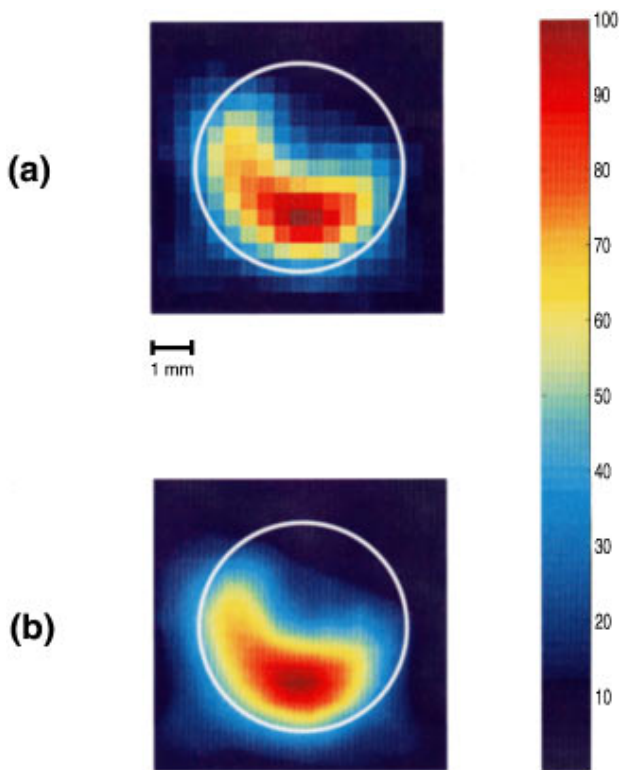


FIG. 4. (a) Raw ^{129}Xe images collected at 1 mT and 0.046 T/m. The image results from 12 angular steps of 30° each. Smoothing this image with a linear, four-point spline interpolation routine produces (b). The white circle in both images represents the 4.8 mm inner diameter of the tube. The spatial resolution is $\sim 950 \mu\text{m}$.

Here, $\pm\Omega_0$ are the resonance frequencies at the opposite ends of the diameter of the tube parallel to the gradient. The center of gravity of $\rho(\Omega)$ in Eq. (1) has been set to zero. A Lorentzian line shape of the form $f(\omega) = (\Delta\omega/2)/\pi[(\Delta\omega/2)^2 + (\omega - \omega_0)^2]$ is assumed, where ω_0 is the center frequency and $\Delta\omega$ is the full width at half-maximum. The convolution of $\rho(\Omega)$ and $f(\omega)$ yields the image:

$$F(\omega) = \int_{-\infty}^{\infty} f(\omega - \Omega)\rho(\Omega)d\Omega. \quad (2)$$

The image is normalized to the peak of the data which are fitted with $\Delta\omega/2\pi = 750$ Hz and $\Omega_0/2\pi = 4.40$ kHz and 3.18 kHz for Figs. 3(a) and 3(b), respectively. The fits are satisfactory, yielding $G = 0.046$ T/m and 0.033 T/m for Figs. 3(a) and 3(b), respectively; the corresponding spatial resolution of the images, $d\Delta\omega/2\Omega_0$, is 500 and 700 μm .

We now demonstrate the feasibility of low-field, SQUID-detected MRI in a solid sample by using polarized solid ^{129}Xe . A two-dimensional (2D) image is obtained by sequentially rotating the cylindrical sample tube in the gradient field applied perpendicularly to its axis, making it possible to reconstruct the distribution of spins in the x - y plane from the radial sampling. The raw 2D image shown in Fig. 4(a) was obtained from 12 sample orientations with 30 free induction decay points per orientation. The 12 separate data sets were collected on the same Xe sample at $B_0 = 1$ mT, corresponding to a Larmor frequency of 11.8 kHz, and $G = 0.046$ T/m. The rf pulses produced a tipping angle of 10° . The white line in Fig. 4 represents the inside wall of the 4.8

mm inner-diameter Pyrex tube containing the solid Xe. A linear, four-point spline interpolation of these data was used to produce the image shown in Fig. 4(b). Evidently the Xe was frozen to one side of the sample tube. From the calibrated gradients and the known 520 Hz linewidth of solid ^{129}Xe in the absence of a gradient¹⁶ we estimate a resolution of $\sim 950 \mu\text{m}$ for the 2D image.

Because the enhanced polarization of the gases will be the same at 300 K as at 4.2 K, we expect the signal to be undiminished for samples at room temperature. Extensions of this technique to room temperature samples using a high- T_c SQUID as a detector are under way. We plan to investigate the dependence of spatial resolution on magnetic field and gradient under these conditions, and to explore the possibility of obtaining images at fields as low as that of the Earth, 0.05 mT.

The authors thank Dr. G. C. Chingas and Dr. T. M. de Swiet for many helpful discussions. This work was supported by the Director, Office of Energy Research, Office of Basic Energy Sciences, Materials Sciences Division, U.S. Department of Energy, under Contract No. DE-AC03-76SF00098. M.P.A. thanks the National Science Foundation Postdoctoral Fellowship Program under Grant No. CHE-9504655. M.T. acknowledges support by the Swiss National Foundation of Science.

¹P. C. Lauterbur, in *NMR in Biology and Medicine*, edited by S. Chien and C. Ho (Raven, New York, 1986).

²P. Mansfield and P. G. Morris, *NMR Imaging in Biomedicine* (Academic, New York, 1982).

³D. G. Gadian, *Nuclear Magnetic Resonance and its Applications to Living Systems* (University Press, Oxford, 1982).

⁴P. T. Callaghan, *Principles of Magnetic Resonance Microscopy* (Clarendon, Oxford, 1991).

⁵S. Kumar, B. D. Thorson, and W. F. Avrin, *J. Magn. Reson., Ser. B* **107**, 252 (1995); S. Kumar, W. F. Avrin, and B. R. Whitcotton, *IEEE Trans. Magn.* **32**, 5261 (1996).

⁶H. C. Seton, D. M. Bussell, J. M. S. Hutchison, and D. J. Lurie, *IEEE Trans. Appl. Supercond.* **5**, 3218 (1995); H. C. Seton, J. M. S. Hutchinson, and D. M. Bussell, *ibid.* **7**, 3213 (1997); *Meas. Sci. Technol.* **8**, 198 (1997).

⁷A. Kastler, *J. Phys. Radium* **11**, 22 (1950).

⁸M. A. Bouchiat, T. R. Carver, and C. M. Varnum, *Phys. Rev. Lett.* **5**, 373 (1960).

⁹R. J. Knize, Z. Wu, and W. Happer, *Adv. At. Mol. Phys.* **24**, 223 (1989).

¹⁰M. S. Albert, G. D. Cates, B. Driehuys, and W. Happer, *Nature (London)* **370**, 199 (1994).

¹¹G. Navon, Y.-Q. Song, T. Room, S. Appelt, R. E. Taylor, and A. Pines, *Science* **271**, 1848 (1996).

¹²Y.-Q. Song, H. D. Gaede, T. Pietraß, G. A. Barrall, G. C. Chingas, M. R. Ayers, and A. Pines, *J. Magn. Reson. Ser. A* **115**, 127 (1995).

¹³H. Middleton, R. D. Black, B. Saam, G. D. Cates, G. P. Cofer, R. Günther, W. Happer, L. W. Hedlund, G. A. Johnson, K. Juvan, and J. Swartz, *Magn. Reson. Med.* **33**, 271 (1995).

¹⁴S. D. Swanson, M. S. Rosen, B. W. Agranoff, K. P. Coulter, R. C. Welsh, and T. E. Chupp, paper presented at the 38th Experimental Nuclear Magnetic Resonance Conference, Orlando, FL, 1997.

¹⁵P. Bachert, L. R. Schad, M. Bock, M. V. Knopp, M. Ebert, T. Großman, W. Heil, D. Hofmann, R. Surkau, and E. W. Otten, *Magn. Reson. Med.* **36**, 192 (1996).

¹⁶D. M. TonThat, M. Ziegeweid, Y.-Q. Song, E. J. Munson, S. Appelt, A. Pines, and J. Clarke, *Chem. Phys. Lett.* **272**, 245 (1997).

¹⁷D. M. TonThat and J. Clarke, *Rev. Sci. Instrum.* **67**, 2890 (1996).

¹⁸E. L. Hahn, *Phys. Rev.* **80**, 580 (1950).

¹⁹B. Saam, N. Drukker, and W. Happer, *Chem. Phys. Lett.* **263**, 481 (1996).

²⁰P. T. Callaghan, A. Coy, L. Ford, and C. Rofe, *J. Magn. Reson., Ser. A* **101**, 347 (1993).

²¹T. M. de Swiet, *J. Magn. Reson., Ser. B* **109**, 12 (1995).